Deep metallic interdiffusion in a model ferromagnetic/molecular system

Cynthia Fourmental,[1,2] Amandine Bellec,[1,*] Vincent Repain,[1] Jérôme Lagoute,[1] Cyril Chacon,[1] Yann Girard,[1] Sylvie Rousset,[1] Yannick J. Dappe,[3] Alina Vlad,[2] Andrea Resta,[2] Yves Garreau,[1,2] and Alessandro Coati[2]

[1]*Université de Paris, Laboratoire Matériaux et Phénomènes Quantiques, CNRS, F-75013 Paris, France*

[2]*Synchrotron SOLEIL, L'orme des Merisiers, Saint-Aubin-BP48,91192 Gif-sur-Yvette Cedex, France*

[3]*SPEC, CEA, CNRS, Universite Paris-Saclay, CEA Saclay, 91191 Gif-sur-Yvette Cedex, France*

(Received 11 March 2019; published 26 August 2019)

Understanding the structure of ferromagnetic/molecular interfaces obtained by the deposition of metal on a molecular layer is a key parameter to master for the development of molecular spintronic devices. Here we studied by means of grazing incidence x-ray diffraction and x-ray reflectivity a model $Co/C_{60}/Co(0001)$ system. Prior to Co deposition, the grown C_{60} layer is crystallized in a face centered cubic lattice with the presence of two twins. The Co overlayer, presenting a polycrystalline hexagonal close packed structure with stacking faults, induces an amorphization of the topmost C_{60} layers. Most importantly, we observe a deep diffusion of Co atoms in the octahedral sites of the crystallized C_{60} film which could strongly affect the spin transport properties of the molecular layer and thus the magnetoresistance of the final device.

DOI: 10.1103/PhysRevMaterials.3.083603

I. INTRODUCTION

The use of organic molecules in spintronic devices has attracted a lot of interest in the past years as they combine the possibility to be tuned at will along with the presence of light elements presenting potentially long diffusion spin lifetime [1]. But it quickly appears that the properties of devices composed of molecular and metallic layers are governed by the interfaces between the molecules and the metallic electrodes [2]. Indeed, the molecules are impacting at the atomic scale the polarization of the hybrid interfaces [3–5] as well as their magnetic properties [6]. Spin dependent hybridization of the molecular orbitals can be generated [7] and interfacial magnetoresistance effects can also be created [8]. The raising "spinterface" field mainly focuses on tuning molecule/ferromagnetic interfaces to induce new functionalities [9,10] that eventually could be controlled by external stimuli [11–13].

For the fabrication of organic spin valves and magnetic tunnel junctions, a lot of effort have been devoted to control the growth of the molecular layer [12,14,15] as the deposition of the second metallic electrode [16,17]. Indeed, the deposition of metal on soft molecular materials can lead to the formation of an "ill-defined" layer containing metallic inclusion [18–20] or metallic filaments [21,22] as well as the formation of new chemical moeties [23,24], which drastically affect the contact resistance [25], spin injection, and transport in the device. If the penetration of metal can be reduced, there are still open questions concerning the interdiffusion process.

In this work we focus our study on a model crystalline system composed of $Co/C_{60}/Co(0001)$. We use grazing incidence x-ray diffraction (GIXD), which is a powerful tool to investigate crystalline systems, to determine the structure of a thin layer of C_{60} molecules grown on a Co(0001) single crystal before and after Co top deposition. We demonstrate that the Co deeply penetrates in the C_{60} crystal and acquires a periodic organization in the whole molecular crystal that has never been evidenced yet.

II. METHODS

To grow the $Co/C_{60}/Co(0001)$ samples, the Co(0001) single crystal was first cleaned under ultrahigh vacuum (UHV) by sputtering (Ar^+ at 900 eV) and annealing (330 °C, 1 h) cycles. The annealing temperature was adapted to avoid the martensitic phase transition around 420 °C [26]. Then the C_{60} molecules were sublimated from a crucible at a temperature of 360 °C on the Co substrate kept at room temperature. Finally, the Co overlayer was deposited by electron assisted deposition. As shown by reflectivity measurements discussed below, the investigated sample presents a C_{60} layer thickness of 170 Å and a Co overlayer thickness of 60 Å, which are typical layer thicknesses used for organic spin valves [27].

The x-ray scattering experiments were carried out on the SixS beamline at SOLEIL synchrotron. The UHV end station is composed of a preparation chamber in which the cleaning cycles and the C_{60} deposition were realized and a main chamber coupled with a $(4+3)$-circle diffractometer where the Co overlayer was grown. All the measurements were performed with an incident beam energy of 18.5 keV and a point detector was used to measure the scattered intensity. All the results presented in the following refer to the hexagonal lattice of the Co(0001) substrate ($\|\vec{a}\| = \|\vec{b}\| = 2.5074$ Å, $\|\vec{c}\| = 4.0699$ Å, $\alpha = \beta = 90°$, $\gamma = 120°$) [28]. For the small q values (<0.4 Å^{-1}), the x-ray reflectivity measurements are fitted using GenX software [29] based on Parratt algorithm [30].

Structural and energetic calculations have been performed using the density functional theory (DFT) code in localized

*amandine.bellec@univ-paris-diderot.fr

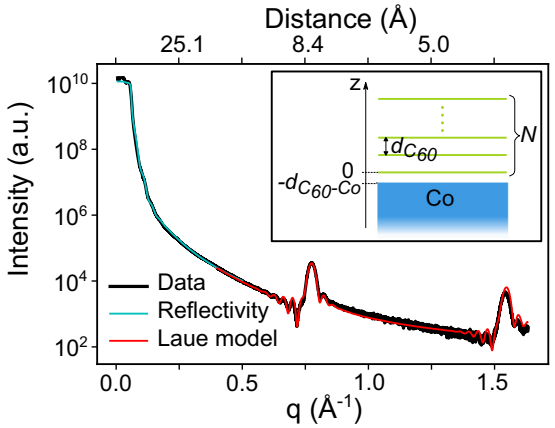

FIG. 1. Reflectivity curve (black) of the C_{60}/Co(0001) sample corrected by geometrical factors [36]. For small q values, the fitted reflectivity curve (blue) is superimposed. For large q values, the superimposed fitting curve (red) is extracted from our developed model to reproduce the Laue oscillations (see main text). In the inset a schematic of the model used, considering N C_{60} layers (in green) separated by $d_{C_{60}}$ and deposited on the Co semi-infinite crystal (in blue) is presented.

orbital basis set Fireball [31]. Standard minimal basis sets for C and Co have been used, following a previous study [32]. To take into account the van der Waals forces in this system, we have used the so-called LCAO-S^2 + vdW approximation to determine the corresponding energy [33]. This approximation is based on the evaluation of the small wave function overlaps between the interacting systems, and the dipole-dipole interaction for the pure van der Waals interaction between those systems, both contributions being treated in perturbation theory. As a result, the sum of these two contributions yields the cohesion energy of the interacting system. This formalism has already proven to give results in good agreement with experiments for graphitic materials and molecules on surfaces [34,35].

III. RESULTS AND DISCUSSION

A. C_{60} growth on Co(0001)

We first discuss the structural properties of the C_{60} layer before discussing their modification by the deposition of the Co overlayer and the induced diffusion of Co atoms in the crystallized C_{60} layer.

Figure 1 presents the reflectivity measurement of the thin C_{60} layer grown on Co(0001). For small q values, the signal quickly decreases. At larger q values, the first and second order diffraction peaks of the C_{60} layer—measured at $q = 0.775$ Å^{-1} and $q = 1.542$ Å^{-1}, respectively—are surrounded by oscillations due to interferences on the different molecular planes called Laue oscillations. Their shape strongly depends on the distance ($d_{C_{60}\text{-Co}}$) between the molecular film and the Co substrate.

For small q values (<0.4 Å^{-1}), the reflectivity curve fit allows us to determine that the C_{60} film has a thickness of 165 ± 15 Å, considering a rough C_{60}/Co interface (see Fig. S1 and Table S1 in the Supplemental Material (SM) [37] for the parameters used). To fit the Laue oscillations, we build a model that calculates the scattered signal from an average number of C_{60} planes (N) separated by a distance $d_{C_{60}}$ on a semi-infinite Co substrate (see inset of Fig. 1). The model is explained in detail in the SM [37]. The asymmetry of Laue oscillations is strongly sensitive to the distance between the Co substrate and the first C_{60} layer called $d_{C_{60}/Co}$. Fitting our data, we extracted an average number of C_{60} planes of 21, a distance between C_{60} planes of 8.154 ± 0.001 Å and a C_{60}/Co distance of 4.90 ± 0.01 Å (see Table S.2 for all the fitting parameters [37]). Considering the spinterfacial properties, the precise determination of the $d_{C_{60}/Co}$ distance, as measured here, is of great importance to further determine the molecule/substrate hybridization. The interplanar distance obtained is smaller by 0.53% than the (111) reticular distance in the fcc C_{60} bulk crystal (8.1973 Å is expected [38]). Comparing the thickness measured at small q values (165 ± 15 Å) to the model for larger q ($21 \times 8.154 = 171 \pm 12$ Å), we can deduce that the full C_{60} layer is well crystallized, which should favor better transport properties [14,15] while minimizing the Co penetration [17].

To characterize the structure of the C_{60} film in the plane parallel to the substrate surface, we measured (h, k) maps of the reciprocal space in grazing incidence geometry and scanning tunneling microscopy topographies (see Fig. S.3 [37]). We thus evidenced that the C_{60} molecules are arranged in close packed hexagonal planes presenting a 4×4 reconstruction with respect to Co(0001). This is in agreement with a crystallization of the C_{60} molecules in a fcc structure with a (111) orientation. Indeed, in the dense (111) plane, the distance between two neighbor molecules is $a_{C_{60}}/\sqrt{2} = 10.0396$ Å [38], which almost exactly corresponds to four times the lattice parameter of the hexagonal close packed (hcp) Co crystal ($a_{Co} = 2.5074$ Å [28]).

To investigate the out-of-plane structure of the C_{60} thin layer, we performed l scans along the (0.25, 0, l), (0.5, 0, l), and (0.75, 0, l) C_{60} rods. The measured C_{60} rods are located at fractional (h, k) coordinates due to the 4×4 periodicity of the molecular layer in the surface plane. As can be seen in the Fig. 2(a), several peaks are observed in the l scans. The representation of the reciprocal space in Fig. 2(b), corresponding to a (h, l) plane at a fixed k value of 0, helps to understand the assignation of each measured peaks. In the scheme, the gray dots represent the position of the expected Bragg peaks of the Co(0001) substrate. The C_{60} thin film crystallizing in a fcc structure with a (111) orientation, as experimentally observed, the reciprocal lattice is therefore a center cubic structure with its [111] direction aligned along the [0001] Co direction. The C_{60} layer can adopt two fcc stackings ABC or CBA, which in the reciprocal space leads to two series of peaks being symmetric from one another by a mirror operation with respect to the [111] C_{60} direction. The two possible twins are represented in Fig. 2(b) by the green and blue dots. The common peaks to both twins are represented by turquoise dots. In the scheme, the directions of the l scans shown in Fig. 2(a) are represented by the solid black, red, and blue lines. Comparing to the reciprocal space scheme, all the peaks measured in the l scan can be assigned to the fcc C_{60} structure. Surprisingly, some expected peaks are missing at the position marked by the blue arrows. This can be understood by looking at the scattering factor of the

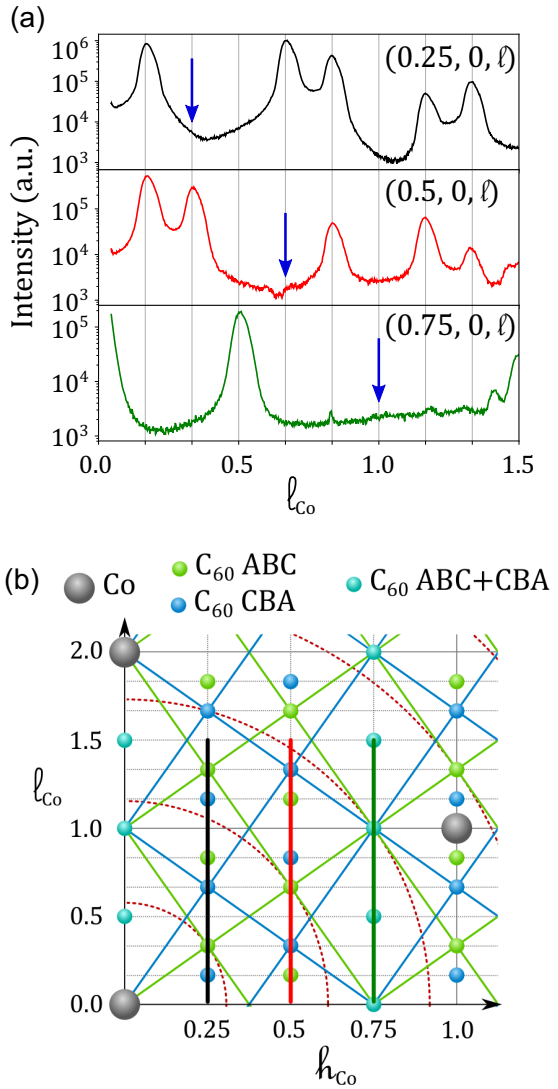

FIG. 2. (a) l scans along the (0.25, 0, l), (0.5, 0, l), and (0.75, 0, l) C_{60} rods in black, red, and green, respectively. The blue arrows indicate the position of extinguished peaks. (b) (h, l) plane scheme of the reciprocal space with the Co lattice in gray and the C_{60} lattice twins in blue and green. The red circles indicate the expected zeros of the C_{60} scattering factor. The solid lines represent the position of the measured C_{60} rods with the same color code as in (a).

C_{60} molecule itself, taking into account a random orientation of the molecules [39], for which zeros are expected at specific q values (see Fig. S.2 [37]) that are marked by the red dotted circles in the reciprocal space scheme. It appears that zeros of the C_{60} scattering factor are located at the q values of the fcc extinguished peaks.

To summarize, we can state that the thin C_{60} layer is well crystallized in a fcc structure with the presence of two twins (ABC and CBA stackings) along the (111) orientation.

B. Co overlayer and deep Co diffusion

We then investigated the growth of a Co overlayer on the molecular thin film. After Co deposition, we measured the reflectivity curve presented in Fig. 3(a) where a clear modification of the oscillations is observed. One can see that

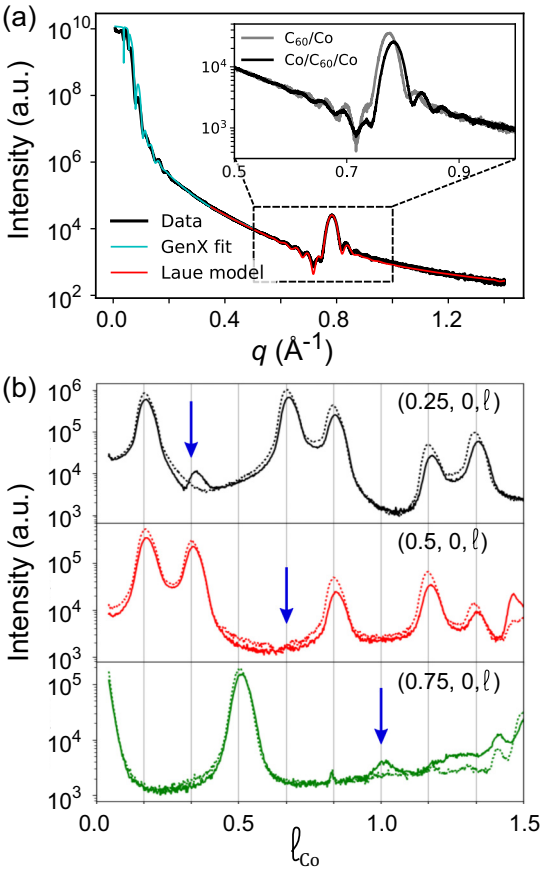

FIG. 3. (a) Experimental reflectivity curve (black) on $Co/C_{60}/Co(0001)$ sample corrected by geometrical factors [36]. The fitting curves at small q values obtained by GenX program (blue curve) and at larger q values obtained by our model (red curve) are superimposed. In the inset, the comparison with the reflectivity curve prior to the Co overlayer deposition (gray curve) is made. (b) l scans along the (0.25, 0, l), (0.5, 0, l), and (0.75, 0, l) C_{60} rods after the deposition of the Co overlayer (solid lines). The l scans recorded prior to the Co deposition are indicated by dotted lines.

the position of the C_{60} diffraction peak is shifted towards a larger q value, indicating a contraction of the C_{60} lattice parameter in the vertical direction. From the fit of the first part of the curve ($q < 0.4$ Å^{-1}), we deduced the Co overlayer thickness of 61 ± 6 Å. Upon the Co deposition, the C_{60} film thickness slightly decreases to 160 ± 15 Å (see Table S.1 [37]). To fit the Laue oscillations, we allow an exponential compression of the topmost C_{60} interplanar distances. By fitting our data, we extracted an average number of C_{60} planes of 18 with an interplanar distance of 8.107 ± 0.001 Å (interplanar distance in the C_{60} layer and near the bottom interface). All the fitting parameter values can be found in the SM [37] (Table S.2) where we also discuss two limit sets of parameters for our model (Fig. S.4 [37]). From this model, we can extract a crystallized layer thickness of 136 ± 14 Å, which is smaller to the C_{60} thickness obtained by the reflectivity measurement. This indicates that part of the C_{60} layer (around three monolayers) is not crystallized anymore as it does not contribute to the Laue oscillation signal. In addition to the

amorphization of the outer C_{60} layers at the top interface, the deposition of the Co overlayer induces a contraction of the interplanar distance of 0.6% in the crystallized C_{60} layer. The contraction is even larger for the external C_{60} planes with an interplanar distance down to 7.3 Å (strong contraction of 10% for the topmost layer). Surprisingly, the contraction gradient quickly decreases to reach a limit interplanar distance value of 8.107 ± 0.001 Å after three layers. This indicates an homogenous contraction over the 15 inner crystallized layers (the crystallized film in contact with the bottom electrode). For its part, the Co overlayer has a polycrystalline hcp structure with stacking faults (see Fig. S.5 [37]).

Figure 3(b) presents the l scans measured for three different C_{60} rods after the Co overlayer deposition. Comparing to the l scans prior to the Co deposition [dotted lines in Fig. 3(b)], one can see a slight shift of the peaks towards larger l values, which confirms the contraction of the (111) interplanar distance in the C_{60} film. In addition, at the position of the C_{60} scattering factor zeros [blue arrows in Fig. 3(b)], new peaks are present at (0.25, 0, 0.33) and (0.75, 0, 1), while still no intensity is measured at (0.5, 0, 0.67). This behavior cannot be explained by the interplanar contraction of the C_{60} film. Indeed, the observed q value decrease does not significantly modify the position of the C_{60} scattering factor zeros (see the SM [37]).

One possibility to explain these modifications is to consider the diffusion of Co atoms into the C_{60} layer and their stabilization into interstitial sites of the fcc C_{60} structure. We therefore calculate the structure factor in the two cases in which Co atoms occupy tetrahedral or octahedral interstitial sites of the C_{60} crystal. In the following the structure factor will be written in the fcc C_{60} lattice. The three measured C_{60} rods indexed (0.25, 0, 0.33), (0.5, 0, 0.67), and (0.75, 0, 1) in the Co lattice are indexed $(2, 0, 0)_{C_{60}}$, $(4, 0, 0)_{C_{60}}$, and $(6, 0, 0)_{C_{60}}$ in the C_{60} lattice, respectively. If positioned in the tetrahedral sites, the Co atoms will give an extra term to the structure factor equal to $\alpha_T f_{Co} \cos[\frac{\pi}{2}(h_{C_{60}} + k_{C_{60}} + l_{C_{60}})]$. While positioned in a octahedral site, the extra term is $\alpha_O f_{Co}(-1)^{(h_{C_{60}}+k_{C_{60}}+l_{C_{60}})}$. $\alpha_{T/O}$ and f_{Co} are the occupation rate in tetrahedral (T) and octahedral sites (O) and the Co scattering factor, respectively. As discussed in the SM [37] (Fig. S.6), one can estimate the intensity evolution of the three $(2, 0, 0)_{C_{60}}$, $(4, 0, 0)_{C_{60}}$, and $(6, 0, 0)_{C_{60}}$ peaks depending on the insertion site of the Co. For Co atom in the tetrahedral sites, the intensity of the three peaks will increase in the same manner. On the contrary, for Co in the octahedral sites, $(2, 0, 0)_{C_{60}}$ and $(6, 0, 0)_{C_{60}}$ peak intensities will vary similarly while the $(4, 0, 0)_{C_{60}}$ peak intensity has a slower evolution. Thus only the presence of Co in the octahedral sites can explain the increase of the $(2, 0, 0)_{C_{60}}$ and $(6, 0, 0)_{C_{60}}$ peaks while the $(4, 0, 0)_{C_{60}}$ is still absent. More quantitatively, as the intensity of the peaks in the l scans is proportional to the scattering factor and consequently to the occupation rate of the interstitial sites, we measured the ratio between neighbor peak intensities. From this ratio, we estimate an occupation rate of the octahedral sites (α_O) of $14 \pm 8\%$ (average value over the crystallized layer).

Ab initio calculations have been performed to simulate the influence of Co atom insertion in both sites on the structural and the energetic properties of the C_{60} crystal.

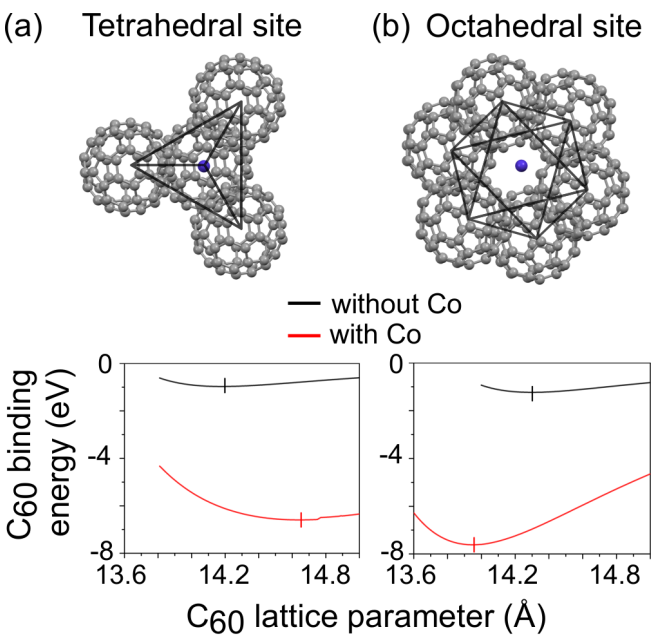

FIG. 4. (a) and (b) Unit cell and calculated C_{60} binding energy as a function of the C_{60} fcc lattice parameter for a tetrahedral (a) and an octahedral (b) sites. The unit cells are oriented along the C_{60} [111] direction (C atoms in gray and Co atoms in blue). The calculations are done with (red curves) and without (black curves) a Co atom inside the sites.

To do so, we have considered two different unit cells. To describe the tetrahedral site, the first cell is composed of four C_{60} molecules positioned at the extremities of an equilateral tetrahedron with a cobalt atom in the center [Fig. 4(a)]. To describe the octahedral site, the second cell is composed of six C_{60} molecules centered on the faces of a cube with a cobalt atom in its center [Fig. 4(b)]. We have then varied the intermolecular distances, leaving the cobalt atom in the center of the cell, and calculated the corresponding energy. This variation has then been compared to the same calculations without cobalt atom in the center of the sites. As can be seen in Fig. 4, inserting a Co atom in the octahedral (tetrahedral) site leads to a compression (expansion) of the C_{60} cell. Thus the measured compression is explained by the deep diffusion of Co in the octahedral sites in the whole Co layer. Considering a homogenous compression of the fcc C_{60} cell, the *ab initio* calculation gives a volume decrease of 7.7%. Supposing that the contraction determined from the reflectivity fitting is only due to the insertion of the Co atoms in the octahedral sites we can estimate an occupation rate α_O for the topmost layers that are strongly compressed and for the inner layers that are undergoing a homogenous compression. The compression of the first topmost layer leads to the full saturation of the octahedral sites (i.e., all of them are occupied by Co atoms), while an occupation rate of 50% is found for the second topmost layer. Experimentally, the limit compression measured is 0.6%, from which we can estimate an occupation rate α_O of 8% in good agreement with the value found experimentally. Surprisingly our data indicated that the Co atoms diffuse deeply in the C_{60} layer with an homogenous distribution. Indeed, as discussed in the SM [37]

(Fig. S.4), the possibility that the Co atom concentration is strong in the topmost layers but that their diffusion until the bottom interface is prevented is not in agreement with the experimental data. The estimated occupation rate corresponds to an average distance between two Co atoms of 120 Å, which is much smaller than the reported spin diffusion length for the C_{60} [40]. Thus the presence of Co will have a strong influence on the spin dependent transport in the C_{60} layer.

IV. CONCLUSIONS

To summarize, we characterized the structure of both spinterfaces of a model Co/C_{60}/Co(0001) system. We show the possibility to grow on Co(0001) well crystallized C_{60} thin films that are having fcc structure. Two twins are observed revealing the presence of both ABC and CBA stackings. At the bottom interface, the distance between the Co and the C_{60} is precisely determined. The growth of a Co overlayer, which presents a hcp structure with stacking faults, strongly affects the C_{60} films as the outer layers become amorphous. More importantly, we show the deep diffusion of atomic Co in the octahedral sites of the whole C_{60} crystal with at least around 10% of occupied sites. The presence of Co in the molecular layer can have a strong influence on the spin dependent transport of electrons in the layer.

ACKNOWLEDGMENTS

The authors thank the French National Research Agency ANR (ANR-BLANC-12 BS10006, SPIROU project), C'Nano / Nano K METEOR, and the European Union's Horizon 2020 research and innovation program under grant agreement No. 766726 for support. We acknowledge SOLEIL for provision of synchrotron radiation facilities and we would like to thank the beamline staff for assistance in using beamline SixS.

[1] V. A. Dediu, L. E. Hueso, I. Bergenti, and C. Taliani, Nat. Mater. **8**, 707 (2009).
[2] C. Barraud, P. Seneor, R. Mattana, S. Fusil, K. Bouzehouane, C. Deranlot, P. Graziosi, L. Hueso, I. Bergenti, V. Dediu, F. Petroff, and A. Fert, Nat. Phys. **6**, 615 (2010).
[3] J. Brede, N. Atodiresei, S. Kuck, P. Lazić, V. Caciuc, Y. Morikawa, G. Hoffmann, S. Blügel, and R. Wiesendanger, Phys. Rev. Lett. **105**, 047204 (2010).
[4] N. Atodiresei, J. Brede, P. Lazić, V. Caciuc, G. Hoffmann, R. Wiesendanger, and S. Blügel, Phys. Rev. Lett. **105**, 066601 (2010).
[5] A. Bedoya-Pinto, S. G. Miralles, S. Vélez, A. Atxabal, P. Gargiani, M. Valvidares, F. Casanova, E. Coronado, and L. E. Hueso, Adv. Funct. Mater. **28**, 1702099 (2018).
[6] K. Bairagi, A. Bellec, V. Repain, C. Chacon, Y. Girard, Y. Garreau, J. Lagoute, S. Rousset, R. Breitwieser, Y.-C. Hu, Y. C. Chao, W. W. Pai, D. Li, A. Smogunov, and C. Barreteau, Phys. Rev. Lett. **114**, 247203 (2015).
[7] S. L. Kawahara, J. Lagoute, V. Repain, C. Chacon, Y. Girard, S. Rousset, A. Smogunov, and C. Barreteau, Nano Lett. **12**, 4558 (2012).
[8] K. V. Raman, A. M. Kamerbeek, A. Mukherjee, N. Atodiresei, T. K. Sen, P. Lazić, V. Caciuc, R. Michel, D. Stalke, S. K. Mandal, S. Blügel, M. Münzenberg, and J. S. Moodera, Nature (London) **493**, 509 (2013).
[9] M. Galbiati, S. Tatay, C. Barraud, A. V. Dediu, F. Petroff, R. Mattana, and P. Seneor, MRS Bull. **39**, 602 (2014).
[10] M. Cinchetti, V. A. Dediu, and L. E. Hueso, Nat. Mater. **16**, 507 (2017).
[11] S. Liang, H. Yang, H. Yang, B. Tao, A. Djeffal, M. Chshiev, W. Huang, X. Li, A. Ferri, R. Desfeux, S. Mangin, D. Lacour, M. Hehn, O. Copie, K. Dumesnil, and Y. Lu, Adv. Mater. **28**, 10204 (2016).
[12] X. Sun, A. Bedoya-Pinto, Z. Mao, M. Gobbi, W. Yan, Y. Guo, A. Atxabal, R. Llopis, G. Yu, Y. Liu, A. Chuvilin, F. Casanova, and L. E. Hueso, Adv. Mater. **28**, 2609 (2016).
[13] G. Molnár, S. Rat, L. Salmon, W. Nicolazzi, and A. Bousseksou, Adv. Mater. **30**, 1703862 (2018).
[14] J. H. Shim, K. V. Raman, Y. J. Park, T. S. Santos, G. X. Miao, B. Satpati, and J. S. Moodera, Phys. Rev. Lett. **100**, 226603 (2008).
[15] K. V. Raman, S. M. Watson, J. H. Shim, J. A. Borchers, J. Chang, and J. S. Moodera, Phys. Rev. B **80**, 195212 (2009).
[16] A. C. Dürr, F. Schreiber, M. Kelsch, H. D. Carstanjen, and H. Dosch, Adv. Mater. **14**, 961 (2002).
[17] D.-O. Kim, J. W. Choi, and D. R. Lee, J. Magn. Magn. Mater. **401**, 506 (2016).
[18] Z. H. Xiong, D. Wu, Z. V. Vardeny, and J. Shi, Nature **427**, 821 (2004).
[19] T.-N. Lam, Y.-L. Lai, C.-H. Chen, P.-H. Chen, Y.-L. Chan, D.-H. Wei, H.-J. Lin, C. T. Chen, J.-H. Wang, J.-T. Sheu, and Y.-J. Hsu, Phys. Rev. B **91**, 041204(R) (2015).
[20] P.-Y. Cheng, M.-R. Chiang, Y.-L. Chan, Y.-J. Hsu, P.-C. Wang, and D. H. Wei, Appl. Phys. Lett. **104**, 043303 (2014).
[21] D. Sun, E. Ehrenfreund, and Z. Valy Vardeny, Chem. Commun. **50**, 1781 (2014).
[22] R. Breitwieser, P. Campiglio, C. Chacon, V. Repain, R. Nemausat, Y. Girard, J. Lagoute, and S. Rousset, Surf. Sci. **606**, 542 (2012).
[23] Y.-L. Chan, Y.-J. Hung, C.-H. Wang, Y.-C. Lin, C.-Y. Chiu, Y.-L. Lai, H.-T. Chang, C.-H. Lee, Y. J. Hsu, and D. H. Wei, Phys. Rev. Lett. **104**, 177204 (2010).
[24] D. H. Wei, C.-H. Wang, H.-C. Chang, Y.-L. Chan, C.-H. Lee, and Y.-J. Hsu, Appl. Phys. Lett. **101**, 141605 (2012).
[25] J. H. Cho, D. H. Kim, Y. Jang, W. H. Lee, K. Ihm, J.-H. Han, S. Chung, and K. Cho, Appl. Phys. Lett. **89**, 132101 (2006).
[26] C. Houska, B. Averbach, and M. Cohen, Acta Metal. **8**, 81 (1960).
[27] M. Gobbi, F. Golmar, R. Llopis, F. Casanova, and L. E. Hueso, Adv. Mater. **23**, 1609 (2011).

[28] A. Taylor and R. W. Floyd, Acta Crystallogr. **3**, 285 (1950).
[29] M. Björck and G. Andersson, J. Appl. Crystallogr. **40**, 1174 (2007).
[30] L. G. Parratt, Phys. Rev. **95**, 359 (1954).
[31] J. P. Lewis, P. Jelínek, J. Ortega, A. A. Demkov, D. G. Trabada, B. Haycock, H. Wang, G. Adams, J. K. Tomfohr, E. Abad, H. Wang, and D. A. Drabold, Phys. Status Solidi B **248**, 1989 (2011).
[32] P. Yang, D. Li, V. Repain, C. Chacon, Y. Girard, S. Rousset, A. Smogunov, Y. J. Dappe, C. Barreteau, and J. Lagoute, J. Phys. Chem. C **119**, 6873 (2015).
[33] Y. J. Dappe, M. A. Basanta, F. Flores, and J. Ortega, Phys. Rev. B **74**, 205434 (2006).
[34] Y. J. Dappe, J. Ortega, and F. Flores, Phys. Rev. B **79**, 165409 (2009).
[35] M. Švec, P. Merino, Y. J. Dappe, C. González, E. Abad, P. Jelínek, and J. A. Martín-Gago, Phys. Rev. B **86**, 121407(R) (2012).
[36] O. Robach, Y. Garreau, K. Aïd, and M. B. Véron-Jolliot, J. Appl. Crystallogr. **33**, 1006 (2000).
[37] See Supplemental Material at http://link.aps.org/supplemental/10.1103/PhysRevMaterials.3.083603 for the reflectivity fitting parameters, the model developed for fitting Laue oscillations, the in plane organization of the C_{60} molecules on Co(0001), the discussion of the Co diffusion profile in the C_{60} film, the powder diagram of the Co overlayer and the discussion on the variation of the C_{60} peak intensities.
[38] R. M. Fleming, T. Siegrist, P. M. Marsh, B. Hessen, A. R. Kortan, D. W. Murphy, R. C. Haddon, R. Tycko, G. Dabbagh, A. M. Mujsce, M. L. Kaplan, and S. M. Zahurak, MRS Proc. **206**, 691 (1990).
[39] D. André, A. Dworkin, H. Szwarc, R. Céolin, V. Agafonov, C. Fabre, A. Rassat, L. Straver, P. Bernier, and A. Zahab, Mol. Phys. **76**, 1311 (1992).
[40] X. Zhang, S. Mizukami, T. Kubota, Q. Ma, M. Oogane, H. Naganuma, Y. Ando, and T. Miyazaki, Nat. Commun. **4**, 1392 (2013).